Copyright © 1973 American Telephone and Telegraph Company
THE BELL SYSTEM TECHNICAL JOURNAL
Vol. 52, No. 6, July–August, 1973
Printed in U.S.A.

Charge Distribution in Buried-Channel Charge-Coupled Devices

By W. H. KENT

(Manuscript received January 11, 1973)

This paper studies charge distribution in buried-channel charge-coupled devices. Detailed development of a one-dimensional electrostatic model is presented and a numerical solution of the resulting nonlinear potential equations is described. Graphical results show the charge-filling mechanism and the relationship between the oxide-semiconductor interface potential and total free positive charge.

I. INTRODUCTION

This paper describes a numerical determination of the distribution of charge in a one-dimensional model of a buried-channel charge-coupled device (CCD).[1] Several calculations have recently been made of the static potential in CCD's in the *absence* of stored charge.[2–4] In addition, the motion of the stored charge under dynamic conditions has been studied by means of essentially one-dimensional models which do not involve a true knowledge of the distribution of stored charge or the charge-carrying capacity of the CCD.[2,5] However, so far it has not been possible to calculate even the static stored-charge distribution in a two-dimensional model of a buried-channel CCD, much less to follow the motion of this charge under dynamic conditions. In this paper a start is made on the problem by calculating the static distribution of stored charge in a one-dimensional model of a buried-channel CCD. The resulting information on the charge distribution is of interest in itself. However, an additional important objective has been to find numerical techniques which can be extended to the two-dimensional problem.

The paper is divided into three parts. Section I treats the physics of the model and Section III gives numerical results. Section II deals briefly with the numerical techniques used and it may be omitted by the reader without loss of continuity.

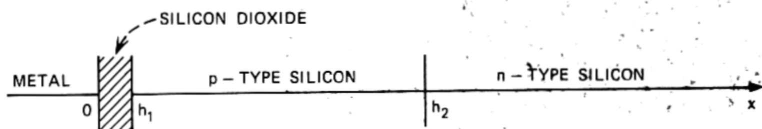

Fig. 1—Buried-channel device structure.

The buried-channel device has a layered structure which will be modeled in one dimension as follows (Fig. 1):

$0 \leqq x \leqq h_1$: silicon dioxide (SiO_2) with relative dielectric constant $\epsilon_1/\epsilon_o = 4$. ($\epsilon_o$ is capacitivity of free space.)

$h_1 \leqq x \leqq h_2$: p-type silicon with acceptor number density $N_A(x)$ and relative dielectric constant $\epsilon_2/\epsilon_o = 12$.

$h_2 \leqq x \leqq \infty$: n-type silicon uniformly doped with constant donor number density N_D and dielectric constant $\epsilon_3 = \epsilon_2$.

The point $x = 0$ is a perfectly conducting boundary held at a potential V_o. The potentials $\phi_1(x)$, $\phi_2(x)$, and $\phi_3(x)$, in the SiO_2, p-type, and n-type regions, respectively, satisfy the one-dimensional Poisson equation,

$$\frac{d^2\phi_i(x)}{dx^2} = -\rho_i(x)/\epsilon_i, \quad i = 1, 2, 3, \tag{1}$$

where the $\rho_i(x)$, the lineal charge densities, are nonlinear functions of the potentials $\phi_i(x)$.

The functional forms of the $\rho_i(x)$ are determined by the assumptions:

(*i*) The SiO_2 is a perfect insulator.

(*ii*) The generation and recombination rates for holes and electrons are zero.

(*iii*) Hole and electron currents are zero at the time of observation.

(*iv*) The flat-band voltage is zero.

(*v*) The injected free holes and electrons are separately in equilibrium.

Conditions (*i*) through (*v*) define a static device for which the $\rho_i(x)$ are:

$$\left.\begin{aligned} \rho_1(x) &= 0, \\ \rho_2(x) &= q[p(x) - N_A(x)], \\ \rho_3(x) &= q[N_D + p(x) - n(x)], \end{aligned}\right\} \tag{2}$$

where $n(x)$ and $p(x)$ are the number densities of free electrons and holes, respectively. The most general expression for $n(x)$ is

$$n(x) = \int_{E_c(x)}^{\infty} g(E)F_e(E)dE, \tag{3}$$

where $g(E)$ is the density of states, $F_e(E)$ is the Fermi distribution for electrons, and $E_c(x)$ is the conduction band edge. Substitution for $g(E)$ and $F_e(E)$ yields

$$n(x) = N_c^o \int_{E_c(x)}^{\infty} \frac{(E - E_c(x))^{\frac{1}{2}} dE}{1 + \exp((E - E_f)/\mathrm{k}T)}. \tag{4}$$

This specific choice for the density of states corresponds to the simplest possible band structure. E_f is the equilibrium Fermi level for electrons and N_c^o is the constant

$$N_c^o = 4\pi(2m_c/\mathrm{h}^2)^{\frac{3}{2}}, \tag{5}$$

where m_c is the effective mass of an electron in silicon and h is Planck's constant.[6]

A similar expression for the distribution of holes is

$$p(x) = \int_{-\infty}^{E_v(x)} g(E) F_h(E) dE, \tag{6}$$

where $F_h(E) = 1 - F_e(E)$; substitution for $g(E)$ and $F_h(e)$ yields

$$p(x) = N_v^o \int_{-\infty}^{E_v(x)} \frac{(E_v(x) - E)^{\frac{1}{2}} dE}{1 + \exp((E_{fh} - E)/\mathrm{k}T)}. \tag{7}$$

$E_v(x)$ is the valence band edge and E_{fh} is defined as the pseudo-Fermi level[7] for the holes. N_v^o is the constant given by

$$N_v^o = 4\pi(2m_v/\mathrm{h}^2)^{\frac{3}{2}}, \tag{8}$$

where m_v is the effective hole mass in silicon.[8] $E_c(x)$ and $E_v(x)$ are functions of $\phi_i(x)$ given by:

$$E_c(x) = E_c^o - q\phi_i(x), \tag{9}$$

$$E_v(x) = E_v^o - q\phi_i(x). \tag{10}$$

E_v^o and E_c^o are the valence and conduction band edges at $x = \infty$, and q is the magnitude of an electronic charge. $p(x)$ and $n(x)$ are functions of the yet undetermined constants E_f and E_{fh}. Later they will appear only in the forms

$$\eta = (E_c^o - E_f)/\mathrm{k}T,$$
$$\eta' = (E_c^o - E_{fh})/\mathrm{k}T.$$

Since only difference terms appear, no energy reference need be established for the model. η will be determined from the electron charge neutrality condition at $x = \infty$. η' is fixed by the total amount of free positive charge $Q_+ = \int_{h_1}^{\infty} p(x)dx$ in the device. In reality, determina-

tion of η' is difficult, so the alternative scheme of choosing η' and calculating the resulting Q_+ is employed. Substituting eqs. (2), (4), and (7) into eq. (1) results in the system of differential equations which characterize the device described above. In the appendix these equations are reduced in a straightforward manner by using the Boltzman approximation; justification for its use is given. The resulting equations which will be solved are ($'$ denotes d/dy):

$$\psi_1''(y) = 0, \qquad 0 \leqq y \leqq h_1/\lambda, \quad (11)$$

$$\psi_2''(y) = \sigma - (m_v/m_c)^{\frac{3}{2}} e^{\rho_o - \psi_2(y)}, \qquad h_1/\lambda \leqq y \leqq h_2/\lambda, \quad (12)$$

$$\psi_3''(y) = e^{\psi_3(y)} - 1 - (m_v/m_c)^{\frac{3}{2}} e^{\rho_o - \psi_3(y)}, \qquad h_2/\lambda \leqq y \leqq \infty, \quad (13)$$

where

$$\psi = q\phi/\mathrm{k}T,$$
$$y = x/\lambda,$$
$$\lambda = \sqrt{\mathrm{k}T\epsilon_2/q^2N_D},$$
$$N_v = N_v^o(\mathrm{k}T)^{\frac{3}{2}},$$
$$N_c = N_c^o(\mathrm{k}T)^{\frac{3}{2}},$$

ϵ_g = the bandgap energy in kT's,

$\eta = (E_c^o - E_f)/\mathrm{k}T$ is a constant dependent on doping levels,

$\eta' = (E_c^o - E_{fh})/\mathrm{k}T$ is a parameter depending on the pseudo-Fermi level,

$$\rho_o = \eta + \eta' - \epsilon_g,$$
$$\sigma = N_A/N_D.$$

m_v and m_c are the effective masses of holes and electrons in silicon; they are $1.08m_o$ and $0.59\ m_o$, respectively.[9] Equations (11), (12), and (13) satisfy boundary conditions

$$\psi_1(0) = V_o \quad (14)$$

and, consistent with eqs. (9) and (10),

$$\psi_3(\infty) = 0. \quad (15)$$

At $y = h_1/\lambda$ and $y = h_2/\lambda$ the continuity conditions are

$$\begin{aligned} \psi_1(h_1/\lambda) &= \psi_2(h_1/\lambda) \\ \epsilon_1\psi_1'(h_1/\lambda) &= \epsilon_2\psi_2'(h_1/\lambda) \end{aligned} \quad (16)$$

$$\begin{aligned} \psi_2(h_2/\lambda) &= \psi_3(h_2/\lambda) \\ \psi_2'(h_2/\lambda) &= \psi_3'(h_2/\lambda). \end{aligned} \quad (17)$$

II. NUMERICAL SOLUTION

The system of differential equations (11), (12), and (13) together with boundary equations (14), (15), (16), and (17) are solved numerically by the method of finite differences.

For computational convenience the length of the device will be truncated from the whole half-line to the segment [0, L]; the distance L is chosen such that $|\psi_3(\infty) - \psi_3(L)|$ and $|\psi_3'(\infty) - \psi_3'(L)|$ are suitably small. [0, L] is partitioned by a mesh of N points and the solution at each point y_i is denoted by ψ^i. The mesh lengths (distance between successive points) are δ_o, δ_p, and δ_n in the oxide, p-region, and n-region, respectively, and are chosen such that $y_{N_1} = h_1/\lambda$ and $y_{N_2} = h_2/\lambda$. The boundaries are $\psi^o = \psi_1(0) = V_o$ and $\psi^N = \psi_3(L) \approx \psi_3(\infty) = 0$. The subscripts on $\psi(y)$ can now be dropped since the superscripts identify the solution point. The second derivative is approximated by the second difference

$$\frac{d^2\psi(y)}{dy^2} = (\psi^{i+1} - 2\psi^i + \psi^{i-1})/\delta^2$$

in each region; δ is one of δ_o, δ_n, or δ_p as appropriate. Using this approximation to discretize eqs. (11), (12), and (13) results in the matrix equation

$$[A][\psi^i] = [\rho(y_i, \psi^i)] \tag{18}$$

which has rows generated by eq. (19); $\rho(y_i, \psi^i)$ is defined in the three regions by the right-hand side of eq. (19).

$$\psi^{i+1} - 2\psi^i + \psi^{i-1} = \begin{cases} 0, & i < N_1, \\ (\sigma - (m_v/m_c)^{\frac{3}{2}} e^{\rho_o - \psi^i})\delta_p, & N_1 < i < N_2, \\ (e^{\psi^i} - 1 - (m_v/m_c)^{\frac{3}{2}} e^{\rho_o - \psi^i})\delta_n, & i > N_2. \end{cases} \tag{19}$$

Rows corresponding to the solutions at the boundary points y_{N_1} and y_{N_2} are obtained from eqs. (16) and (17) where the first derivative is approximated by

$$\mp\psi'(y) \approx (+11\psi(y) - 18\psi(y \pm \delta) + 9\psi(y \pm 2\delta) - 2\psi(y \pm 3\delta))/6\delta, \tag{20}$$

and δ is the appropriate mesh size for each region (the positive or forward derivative uses points to the left of y). Equation (20) results from simultaneous solution of the Taylor expansions for $\psi(y \pm \delta)$, $\psi(y \pm 2\delta)$, and $\psi(y \pm 3\delta)$ with terms $0(\delta^4)$ and higher dropped; the result is accurate to $0(\delta^3)$ which is consistent with the second difference approximation to $d^2\psi/dy^2$. In the oxide layer, a first-difference approximation

$$\psi'(x) = (\psi^i - \psi^{i-1})/\delta_o \tag{21}$$

is adequate since the solution in this region is linear. The boundary equations are:

for $i = N_1$,

$$-(6\delta_p\epsilon_1/\delta_o\epsilon_2)\psi^{N_1-1} + (11 + 6\delta_p\epsilon_1/\delta_o\epsilon_2)\psi^{N_1} - 18\psi^{N_1+1} + 9\psi^{N_1+2} - 2\psi^{N_1+3} = 0; \quad (22)$$

for $i = N_2$,

$$(-1/\delta_p)(2\psi^{N_2-3} - 9\psi^{N_2-2} + 18^{N_2-1}) + 11\psi^{N_2}(1/\delta_n + 1/\delta_p) - (1/\delta_n)(18\psi^{N_2+1} - 9\psi^{N_2+2} + 2\psi^{N_2+3}) = 0. \quad (23)$$

The matrix A in eq. (18) is tridiagonal except for the N_1th and N_2th rows.

For each choice of the parameter ρ_o, the $\{\psi^i\}$ of eq. (18) are solved for iteratively using a combination of successive under- and over-relaxation[10] (SOR) on the equation

$$[\psi^i] = [A]^{-1}[\rho(y_i, \psi^i)]. \quad (24)$$

The procedure described here differs slightly from the usual SOR in that the transformed equation (24) is solved instead of eq. (18). For the ith row of eq. (24), the $j + 1$th estimate of ψ^i is given as

$$\psi^i_{j+1} = \psi^i_j + \omega(\tilde{\psi}^i - \psi^i_j), \quad (25)$$

where ω is a relaxation parameter with values $0 < \omega \leqq 2$. $\tilde{\psi}^i$ is a Newton's method solution of eq. (26), a transcendental equation in ψ^i resulting from the ith row of eq. (24) with the remaining $N - 2$ variables ψ^k held constant. The coefficients a^{-1}_{ik} in eq. (26) are elements of A^{-1}.

$$\psi^i - \sum_{k=1}^{i-1} a^{-1}_{ik}\rho(y_k, \psi^k_{j+1}) - a^{-1}_{ii}\rho(y_i, \psi^i) - \sum_{k=i+1}^{N-1} a^{-1}_{ik}\rho(y_k, \psi^k_j) = 0. \quad (26)$$

Criteria for convergence of the process, as well as the choice of the value of ω, is based on the residual r_j defined at the jth iteration as

$$r_j = \sum_{i=1}^{N-1} |\psi^i_j - \psi^i_{j-1}|. \quad (27)$$

It can be shown that if (18) were a linear system of equations and if ψ^i were the true solution at y_i then

$$\sup_{1 \leqq i \leqq N} |\psi^i - \psi^i_{j+1}| / \sup_{1 \leqq i \leqq N} |\psi^i| \leqq C(\omega) r_{j+1}, \quad (28)$$

where $C(\omega)$ is a constant dependent on the choice of ω.[11] For the optimum value of ω, $C(\omega)$ is $0(N)$ while for values of ω only slightly different

from the optimum $C(\omega)$ can be $0(N^2)$. In the computations presented in the next section, $N \leqq 100$ so the iterative process was stopped when the residual terms were less than 10^{-8}; this allowed margin for the fact that (18) is nonlinear. A discussion of the choice of ω is necessarily even more heuristic. It was found that for a mesh of $N = 50$ points and large negative values of ρ_o corresponding to small positive charge densities (i.e., $e^{\rho_o - \psi^i} \ll 1$ for all i), the iterative scheme was convergent for any choice of ω and any initial estimate of the $\{\psi^i\}$. For less-negative values of ρ_o and the corresponding larger values of $e^{\rho_o - \psi^i}$, the scheme was convergent for over-relaxation ($\omega > 1$) only if $r_j < 10$ for all j (approximate figure); but using under-relaxation the process was well behaved with r_j's as great as 10^4. It should be pointed out that due to the exponential nature of the right-hand side of eq. (19) even a very good initial estimate typically resulted in $r_1 > 10^3$ when over-relaxation was applied. Although the SOR process described above may well be stable[12] regardless of r_j values, the magnitude of the exponential terms in (19) limits machine computations. The combination of under- and over-relaxation detailed below eliminates this problem.

Good initial estimates for the $\{\psi^i\}$ were obtained by choosing the ρ_o values with equal spacing $\Delta\rho$; the first ρ_o value being the small positive charge-density case described above. With $\Delta\rho < 10$ a linear estimate of the $\{\psi^i\}$ for successive values of ρ_o was adequate. The iterations were under-relaxed ($\omega = 0.5$) until the residual term was less than 10; successive iterations were over-relaxed so as to increase the rate of convergence. The choice of ω for the SOR steps was not critical; values in the range $1 < \omega \leqq 1.5$ had approximately the same rate of convergence. Values above 1.5 did not converge for all values of ρ_o.

Total positive charge in the device for a given value of ρ_o is calculated by

$$Q_+ = \int_{y_{N_1}}^{y_{N_2}} e^{\rho_o - \psi_2(y)} dy + \int_{y_{N_2}}^{L} e^{\rho_o - \psi_3(y)} dy. \tag{29}$$

Using a piecewise linear approximation for $\psi(y)$ on $[y_k, y_{k+1}]$,

$$\psi(y) \cong \psi^k + ((y - y_k)/\delta)(\psi^{k+1} - \psi^k), \tag{30}$$

and summing the integrals over each such interval in $[y_{N_1}, L]$ gives the approximation

$$Q_+ \cong \delta_p \sum_{i=N_1}^{N_2-1} e^{\rho_o}(e^{-\psi^i} - e^{-\psi^{i+1}})/(\psi^{i+1} - \psi^i) + \delta_n \sum_{i=N_2}^{N-1} e^{\rho_o}(e^{-\psi^i} - e^{-\psi^{i+1}})/(\psi^{i+1} - \psi^i), \tag{31}$$

which can be modified to include the case $\psi^{i+1} = \psi^i$. Dimensional charge in coulombs can be calculated from Q_+ by $Q = Q_+ N_D \lambda$.

The operational scheme may be summarized as follows:

(*i*) Choose a value of ρ_o corresponding to small total charge Q_+ ($\rho_o \rightarrow -\infty$ in eq. (24) $\Rightarrow Q_+ \rightarrow 0$),
(*ii*) Solve for $\psi(y)$, thus determining $p(y)$,
(*iii*) Integrate $p(y)$ to find Q_+,
(*iv*) Increment ρ_o by $\Delta\rho$ and repeat (*ii*), (*iii*), and (*iv*).

The technique of starting with $Q_+ \approx 0$ and slowly adding positive charge to the device is important since it is this scheme of operation, in conjunction with the successive under- and over-relaxation, that avoids the exponential overflow limitations in machine computation.

III. COMPUTATIONAL RESULTS

In this section, numerical results for two specific device configurations will be given. The first device has a constant doping profile (N_A = a constant) and dimensions

$$h_1/\lambda = 0.48,$$
$$h_2/\lambda = 12.48,$$
$$L = 42.48.$$

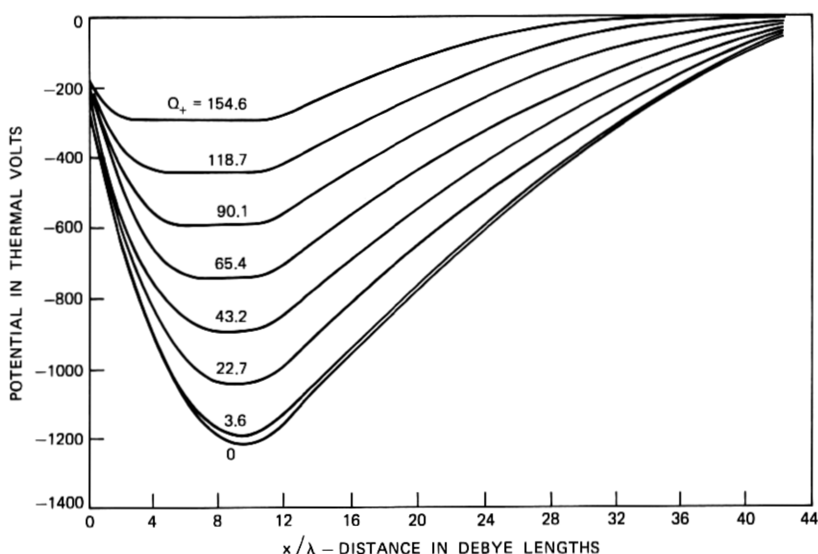

Fig. 2—Potential versus distance for a buried-channel device with uniformly doped p-region and $V_o = -4$ volts.

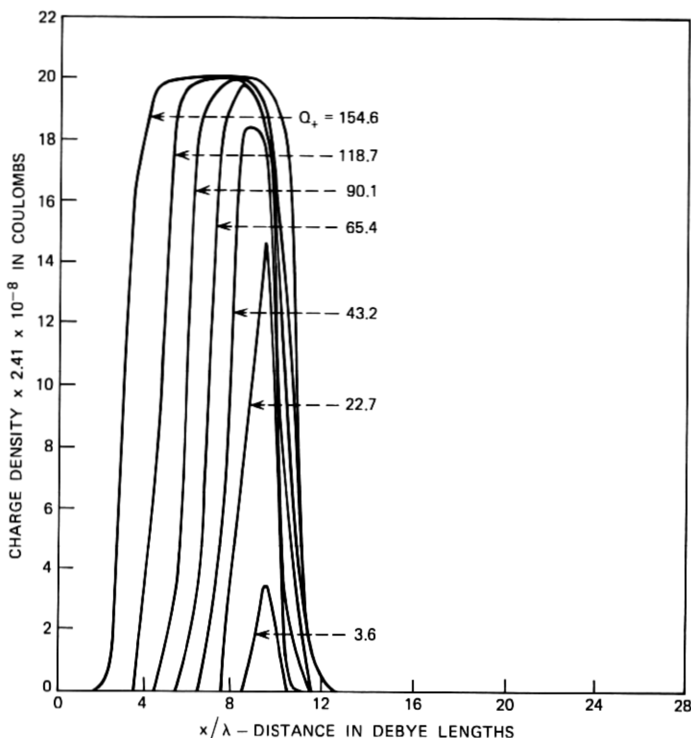

Fig. 3—Charge density versus distance for a buried-channel device with uniformly doped p-region.

λ in this case is approximately 0.415 μm. Doping levels are

$$N_A = 2 \times 10^{15} \text{ cm}^{-3},$$
$$N_D = 1 \times 10^{14} \text{ cm}^{-3},$$

so

$$\sigma = N_A/N_D = 20.$$

N_c is calculated by[13]

$$N_c = 4.831 \times 10^{15}(m_c/m_o)^{\frac{3}{2}}T^{\frac{3}{2}},$$

with $T = 300°\text{K}$ and m_c as before.

Using eq. (46), η is found to be

$$\eta = 12.09.$$

The nondegeneracy condition for this device may now be stated using eq. (45)

$$\epsilon_g - \eta' + \psi(y) > 3.5,$$

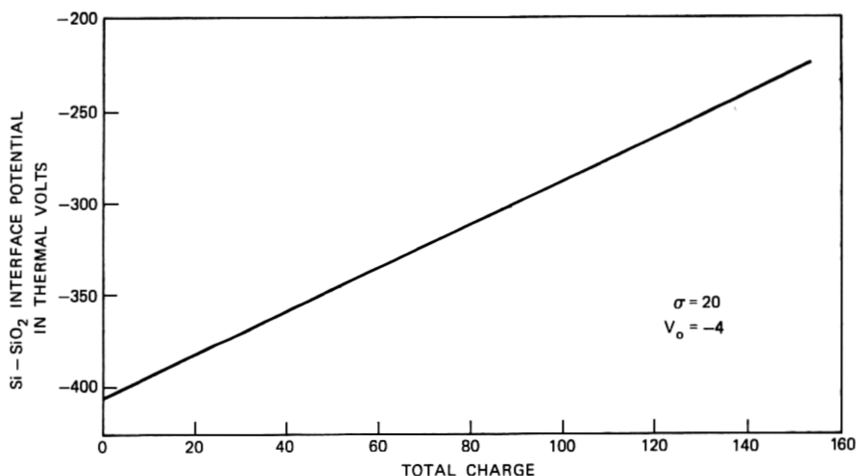

Fig. 4—Potential at the Si-SiO$_2$ interface versus total positive charge in a buried-channel device with a uniform p-region and $V_o = -4$ volts.

or

$$\eta' - \epsilon_g - \psi(y) < -3.5.$$

Adding η to both sides of the inequality gives

$$\rho_o - \psi(y) < \eta - 3.5.$$

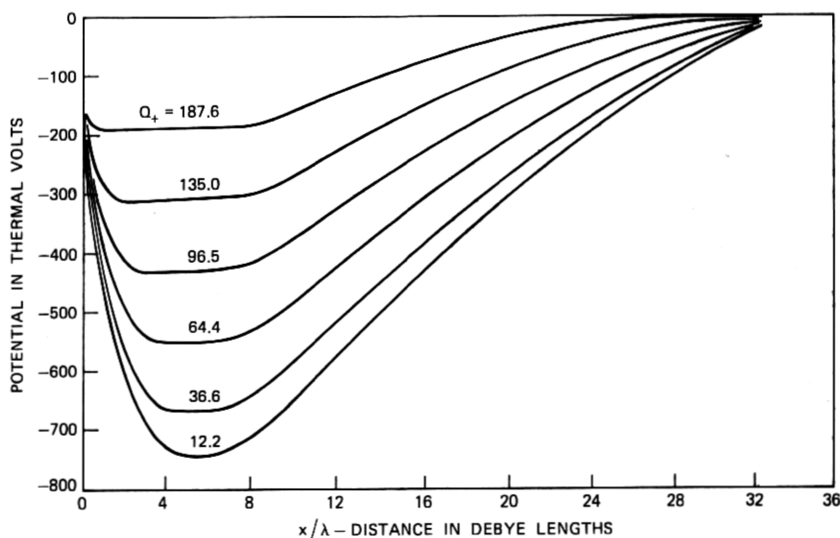

Fig. 5—Potential versus distance for a buried-channel device with a Gaussian p-region doping profile and $V_o = -4$ volts.

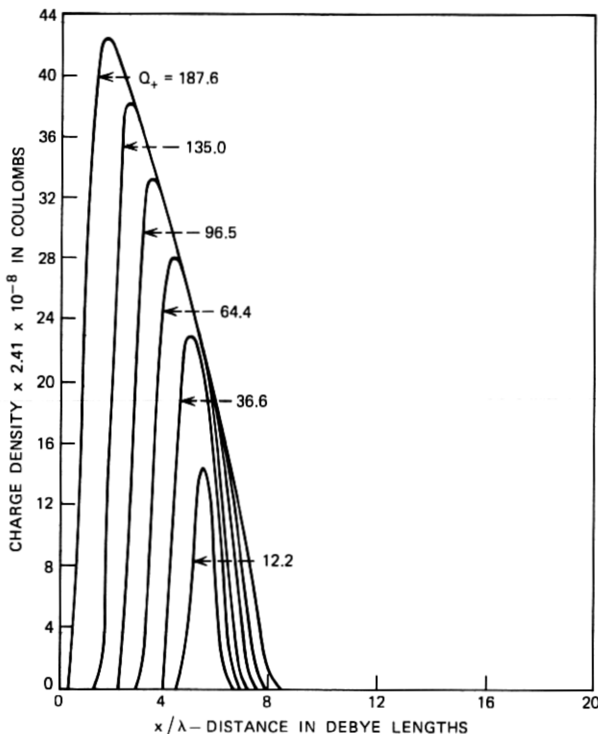

Fig. 6—Charge density versus distance for a buried-channel device with a Gaussian doping profile.

Then for each choice of the parameter ρ_o, the solution set $\{\psi^i\}$ must satisfy:

$$\rho_o - \psi^i < 8.59. \tag{32}$$

From eq. (12) it is clear that if one assumes the Boltzmann approximation to hold, then as long as $Q_+ < \sigma(h_2 - h_1)/\lambda$ the equilibrium condition causes the lineal charge density to have constant sign so

$$\rho_o - \psi^i < \log \sigma(m_c/m_v)^{\frac{3}{2}} \tag{33}$$

for all i; for this device, eqs. (32) and (33) are always consistent if $N_A < 1.3 \times 10^{18}\ \text{cm}^{-3}$.

Computation was performed using a 90-point mesh and took approximately 4.8 minutes of processor time on a Honeywell 6000-series machine.

Figures 2, 3, and 4 summarize the computational results. Figure 2 shows potential solutions $\{\psi^i\}$ versus the points y_i for a family of ρ_o

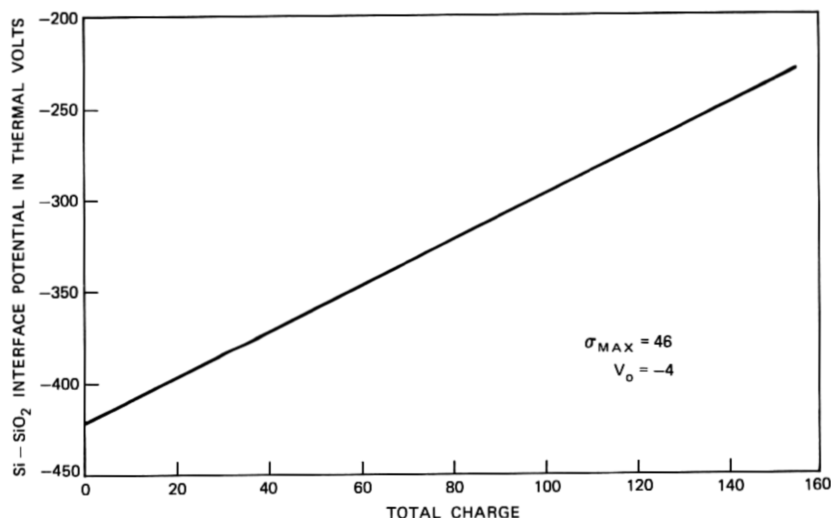

Fig. 7—Potential at the Si-SiO_2 interface versus total positive charge in a buried-channel device with a Gaussian p-region doping profile and $V_o = -4$ volts.

values with $V_o = -4$ volts. The range of total charge values is indicated. Figure 3 is a plot of the linear charge density with Q_+ values indicated. Figure 4 is Q_+ plotted against ψ^{N_1} (the oxide-interface potential).

A realistic modification to the device studied thus far is to allow σ to have y variation. The second set of results presented are for the same device as described above but with the p-region having a doping profile

$$\sigma(y) = (D_s + 1)e^{-[(y-h_1)/(h_2-h_1)]^2 \ln (D_s+1)} - 2. \tag{34}$$

The values for h_1, h_2, and V_o are as before, $L = 32.48$, and $D_s = 46$. [This value of D_s corresponds to an average doping level in the p-layer of $\bar{N}_A = 1.9 \times 10^{15}/\text{cm}^3$, and eq. (34) describes a doping profile as if the p-layer were formed by drive-in diffusion.[14]] The solutions $\{\psi^i\}$ must still satisfy eq. (32). Figures 5, 6, and 7 are a summary of results.

Comparison of the two cases shows that for the doping profile in eq. (34) the potential minimum is greater and the "channel" is shifted toward the oxide. In both cases the added positive charge is contained entirely in the p-region and it fills the region starting from the side remote from the oxide interface (see Figs. 2 and 5).

IV. ACKNOWLEDGMENTS

The work presented here has benefitted from constructive suggestions by N. L. Schryer, G. E. Smith, R. J. Strain, and D. A. Kleinman.

Special thanks goes to J. McKenna for his many contributions during the course of this work and for his comments regarding the preparation of this paper.

APPENDIX

Substituting eqs. (2), (4), and (7) into eq. (1) results in (′ denotes d/dx):

$$\phi_1''(x) = 0, \qquad 0 \leqq x \leqq h_1, \tag{35}$$

$$\phi_2''(x) = \frac{q}{\epsilon_2}\left\{N_A - N_v^o \int_{-\infty}^{E_v(x)} \frac{(E_v(x) - E)^{\frac{1}{2}} dE}{1 + \exp\left[(E_{fh} - E)/\mathrm{k}T\right]}\right\}, \qquad h_1 \leqq x \leqq h_2, \tag{36}$$

$$\phi_3''(x) = \frac{q}{\epsilon_2}\left\{N_c^o \int_{E_c(x)}^{\infty} \frac{(E - E_c(x))^{\frac{1}{2}} dE}{1 + \exp\left[(E - E_f)/\mathrm{k}T\right]} - N_D - N_v^o \int_{-\infty}^{E_v(x)} \frac{(E_v(x) - E)^{\frac{1}{2}} dE}{1 + \exp\left[(E_{fh} - E)/\mathrm{k}T\right]}\right\}, \qquad h_2 \leqq x \leqq \infty. \tag{37}$$

Transform the integral involving $E_c(x)$ by making the substitutions:

$$\epsilon = (E - E_c(x))/\mathrm{k}T,$$
$$E_c(x) = E_c^o - q\varphi(x),$$
$$\eta = (E_c^o - E_f)/\mathrm{k}T.$$

For the integrals involving $E_v(x)$ make the substitutions:

$$\epsilon = (E_v(x) - E)/\mathrm{k}T,$$
$$E_v(x) = E_v^o - q\varphi(x),$$
$$\eta' = (E_c^o - E_{fh})/\mathrm{k}T,$$
$$\epsilon_g = (E_c^o - E_v^o)/\mathrm{k}T.$$

For both cases let

$$\psi(x) = q\varphi(x)/\mathrm{k}T$$

and make the change of variables

$$y = x/\lambda,$$

where

$$\lambda = \sqrt{\mathrm{k}T\epsilon_2/q^2 N_D}.$$

These substitutions and some straightforward manipulation reduce eqs. (35), (36), and (37) to

$$\psi_2''(y) = 0, \qquad 0 \leqq y \leqq h_1/\lambda, \tag{38}$$

$$\psi_2''(y) = \frac{N_A}{N_D} - \frac{N_v^o}{N_D}(\mathrm{k}T)^{\frac{3}{2}} \int_0^{\infty} \frac{\epsilon^{\frac{1}{2}} d\epsilon}{1 + \exp\left(\epsilon + \epsilon_g - \eta' + \psi_2(y)\right)}, \qquad h_1/\lambda \leqq y \leqq h_2/\lambda, \tag{39}$$

$$\psi_3''(y) = \frac{N_c^0}{N_D}(\mathrm{k}T)^{\frac{3}{2}}\int_0^\infty \frac{\epsilon^{\frac{1}{2}}d\epsilon}{1+\exp\left[\epsilon+\eta-\psi_3(y)\right]} - 1$$

$$- \frac{N_v^0}{N_D}(\mathrm{k}T)^{\frac{3}{2}}\int_0^\infty \frac{\epsilon^{\frac{1}{2}}d\epsilon}{1+\exp\left(\epsilon+\epsilon_g-\eta'+\psi_3(y)\right)},$$

$$h_2/\lambda \leqq y \leqq \infty. \quad (40)$$

These equations are further simplified by making the classical Boltzmann approximation for the electrons:

$$\int_0^\infty \frac{\epsilon^{\frac{1}{2}}d\epsilon}{1+\exp\left(\epsilon+\eta-\psi(y)\right)} \cong \int_0^\infty \frac{\epsilon^{\frac{1}{2}}d\epsilon}{\exp\left(\epsilon+\eta-\psi(y)\right)} \quad (41)$$

which holds since $\eta - \psi(y)$ is always positive by several kT (see Fig. 8). The last result is integrable and simplifies the approximation to

$$\Gamma(\tfrac{3}{2})\exp\left(\psi(y)-\eta\right), \quad (42)$$

where $\Gamma(\cdot)$ is the usual gamma function. This approximation has been shown to be less than one percent in error if[15]

$$\eta - \psi(y) > 3.5. \quad (43)$$

Similarly, for the holes,

$$\int_0^\infty \frac{\epsilon^{\frac{1}{2}}d\epsilon}{1+\exp\left(\epsilon+\epsilon_g-\eta'+\psi(y)\right)} \cong \Gamma(\tfrac{3}{2})\exp\left(\eta'-\epsilon_g-\psi(y)\right) \quad (44)$$

if

$$\epsilon_g - \eta' + \psi(y) > 3.5. \quad (45)$$

The validity of this last approximation is not clear since $\psi(y)$ is dependent on η' and $\psi(y)$ becomes large and negative. Note that *requiring* the inequalities (43) and (45) to hold is equivalent to requiring the device to be nondegenerate. Computational results show this approximation to be consistent.

η is expressed in terms of the constants N_c, N_v, and N_D by requiring electron charge neutrality at $x = \infty$. It should be stated that the correct condition to use at this point is complete charge neutrality. This requirement, however, is computationally indistinguishable from the algebraically simpler condition used here. Using eqs. (40) and (15), the neutrality condition is

$$(N_c/N_D)e^{-\eta}\Gamma(\tfrac{3}{2}) - 1 = 0,$$

so

$$N_c/N_D = e^{\eta}/\Gamma(\tfrac{3}{2}). \quad (46)$$

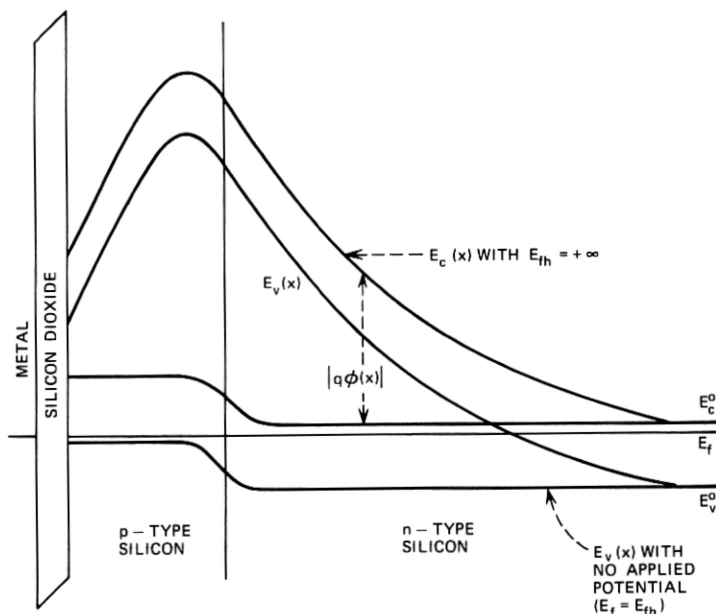

Fig. 8—Band diagram for buried-channel device.

Equation (46) defines the Fermi level for the electrons. Using eqs. (5) and (8),

$$N_v/N_D = (N_v/N_c)\cdot(N_c/N_D) = (m_v/m_c)^{\frac{3}{2}}e^{\eta}/\Gamma(\tfrac{3}{2}), \qquad (47)$$

where m_v and m_c are the effective masses of holes and electrons in silicon; they are 1.08 m_o and 0.59 m_o, respectively.[10] Using eqs. (42), (44), (46), and (47) in eqs. (38), (39), and (40) results in equations (11), (12), and (13) which are to be solved.

REFERENCES

1. Walden, R. H., Krambeck, R. H., Strain, R. S., McKenna, J., Schryer, N. L., and Smith, G. E., "The Buried Channel Charge Coupled Device," B.S.T.J., *51*, No. 7 (September 1972), pp. 1635–1640.
2. Amelio, G. F., "Computer Modeling of Charge-Coupled Device Characteristics," B.S.T.J., *51*, No. 3 (March 1972), pp. 705–730.
3. McKenna, J., and Schryer, N. L., "The Potential in a Charge Coupled Device With No Mobile Minority Carriers and Zero Plate Separation," B.S.T.J., *52*, No. 5 (May-June 1973), pp. 669–696.
4. McKenna, J., and Schryer, N. L., "The Potential in a Charge-Coupled Device With No Mobile Minority Carriers," unpublished work.
5. Strain, R. J., and Schryer, N. L., "A Nonlinear Diffusion Analysis of Charge-Coupled-Device Transfer," B.S.T.J., *50*, No. 6 (July-August), pp. 1721–1740.
6. Blakemore, J. S., *Semiconductor Statistics*, New York: Pergamon Press, 1962, pp. 75–77.

7. Grove, A. S., *Physics and Technology of Semiconductor Devices*, New York: John Wiley and Sons, 1967, p. 162.
8. Blakemore, J. S., op. cit., p. 81.
9. Blakemore, J. S., op. cit., pp. 58–63.
10. Varga, R. S., *Matrix Iterative Analysis*, Englewood Cliffs, N. J.: Prentice-Hall, 1962, p. 59.
11. McKenna, J., unpublished work.
12. Richtmeyer, R. D., and Morton, K. W., *Difference Methods for Initial Value Problems*, 2nd Ed., New York: Interscience, 1970, p. 9.
13. Blakemore, J. S., op. cit., p. 82.
14. Grove, A. S., op. cit., p. 43.
15. Blakemore, J. S., op. cit., p. 358.